J Solid State Electrochem (2003) 7: 337–343
DOI 10.1007/s10008-002-0332-1

ORIGINAL PAPER

Feng Zhao · Lihua Bi · Junguang Jiang · Li Qi
Mingkui Wang · Shaojun Dong

Electrochemical behavior of α-Keggin-type nanoparticles, $Co(en)_3(PMo_{12}O_{40})$, in polyethylene glycol

Received: 28 January 2002 / Accepted: 25 September 2002 / Published online: 25 October 2002

Abstract The electrochemical behavior of α-Keggin-type nanoparticles, $Co(en)_3(PMo_{12}O_{40})$ (abbreviated as PMo_{12}-Co), have been studied in poly(ethylene glycol) for four different molecular weights (PEG, average MW 400, 600, 1000, and 2000 g mol^{-1}) and containing $LiClO_4$ (O/Li = 100/1) supporting electrolyte. The diffusion coefficients of the PMo_{12}-Co nanoparticles were determined using a microelectrode by chronoamperometry for PEG of different molecular weights that were used to describe the diffusion behavior of PMo_{12}-Co nanoparticles in different phase states. Moreover, the conductivity of the composite system increases upon addition of PMo_{12}-Co nanoparticles, which was measured by an a.c. impedance technique. FT-IR spectra and DSC were used to follow the interactions of PEG-$LiClO_4$-PMo_{12}-Co, and well described the reason that the PMo_{12}-Co nanoparticles could promote the conductivity of the PEG-$LiClO_4$-PMo_{12}-Co system.

Keywords Diffusion coefficient · Polyoxometalates · Poly(ethylene glycol) · Nanoparticles · Microelectrode

Introduction

The field of polyoxometalates, though a fruitful field, continues to attract significant attention. Recently, many efforts have centered on the functional hybrid materials of polyoxometalates, especially nano-size hybrid organic-inorganic materials. Conventional macroscopic composite materials have shaped our world, yet, when it comes to the microscopic world, components interact at a molecular level and particle size reduction boosts the importance of the interphase in composite mixtures, the hybrid nanoparticles improve electrical properties, ionic conductivity, luminescence, and so on [1, 2, 3]. These new useful properties and performance of nanoparticles provide an opportunity for investigation of the microscopic world. For example, an increase in conductivity of polymer electrolytes by nanoparticles has been reported [4, 5, 6], but the microscopic mechanism is still under discussion.

However, nanoparticles are poor film formers and they require a carrier matrix to provide the film-forming properties when they are used in display devices, sensors, energy storage applications, etc. Of the many systems examined, poly(ethylene glycol) (PEG) is commonly used as the polymer matrix because of its chemical and electrochemical stability and the ability to dissolve high concentrations of salts to form homogenous polymer electrolytes, which then have the possibility of application in various electrochemical devices [7, 8, 9]. Murray and co-workers [10, 11] have successfully used ferrocene to explore electrochemical and transport phenomena in polymer electrolytes. However, as a fundamental topic, the electrochemical behavior and useful properties of nanoparticles have not been widely studied in polymer electrolytes.

In this work, polymer electrolytes were prepared using PEG of four molecular weights, $LiClO_4$, and α-Keggin-type polyoxometalate nanoparticles, $Co(en)_3$ ($PMo_{12}O_{40}$), with a size of 1–5 nm and abbreviated as PMo_{12}-Co. Different molecular weight PEGs were used to detect the effect of the crystallinity state and amorphous phase state on the nanoparticles' mobility. Because microelectrodes have unique characteristics such as low current and small *IR* drop, they are suitable for exploring reaction mechanisms and the diffusion behavior of ions in highly resistive solvents [12, 13]. In the present work, a microdisk electrode was used to determine the diffusion coefficients of PMo_{12}-Co nanoparticles in the polymer electrolyte with non-steady-state chronoamperometry. An obvious

F. Zhao · L. Bi · J. Jiang · L. Qi · M. Wang · S. Dong (✉)
State Key Laboratory of Electroanalytical Chemistry,
Changchun Institute of Applied Chemistry,
Chinese Academy of Sciences,
Changchun 130022, China
E-mail: dongsj@ciac.jl.cn
Fax: +86-431-5689711

increase in conductivity was observed after the addition of PMo_{12}-Co by a.c. impedance. DSC and FT-IR spectroscopy were used to study the effect of PMo_{12}-Co on ion mobility, conductivity, and PEG-$LiClO_4$-PMo_{12}-Co interactions.

Experimental

Preparation of polymer electrolytes

PEGs (average molecular weights 400, 600, 1000, and 2000 g mol^{-1}) and analytically pure $LiClO_4$ were supplied by Shanghai Chemicals (China). The polyoxometalate nanoparticles of the α-Keggin type, $Co(en)_3(PMo_{12}O_{40})$ (size 1–5 nm), were presented by Prof. Rudan Huang (Northeast Normal University), and were synthesized and characterized as published [14]; $LiClO_4$ and PMo_{12}-Co were dried at 100 °C under vacuum for 48 h before use. The preparation of the polymer electrolyte samples involved first the dispersion of PMo_{12}-Co in PEG by stirring for 10 h, followed by addition of $LiClO_4$ (O/Li = 100/1, molar ratio) under stirring, and heating the resulting mixture. Then all the polymer electrolytes were dried in a vacuum oven at 30 °C for 24 h to remove the residual moisture thoroughly.

Differential scanning calorimetry

DSC of the polymer electrolytes was carried out by slow cooling to –60 °C to stabilize the material, which was then heated from –60 °C to 100 °C at rate of 10 K min^{-1} using a Perkin-Elmer-7 system in a nitrogen atmosphere.

Fourier transform infrared analysis

FT-IR spectra were recorded on a computer-interfaced Nicolet 520 FT-IR spectrometer (USA) with a wavenumber resolution of 4 cm^{-1}. For each FT-IR measurement a small drop of the sample solution was evenly spread onto a KBr pellet.

Electrochemical measurements

All electrochemical experiments, including cyclic voltammetry, chronoamperometry, and a.c. impedance technology, were carried out by an Autolab/PG30 electrochemical analyzer system (ECO Chemie, Netherlands) in an earthed Faraday cage. A 10-μm diameter Pt fiber was used as the working electrode; Pt wire (1 mm) and Ag wire (0.5 mm) were used as the counter electrode and pseudo-reference electrode, respectively. The three electrodes were sealed together in a glass tube by epoxy resin, and then polished with abrasive paper and α-Al_2O_3 powder of 1, 0.05, and 0.03 μm, and finally cleaned in an ultrasonic water bath. The radius of the working electrode was determined voltammetrically from the plot of the steady-state current versus the concentration of $Fe(CN)_6^{3-}$ in 1 M KCl of known diffusion coefficient. Before cyclic voltammetry and chronoamperometry measurements, the glass container of the polymer electrolytes was purged with dry argon gas for 10 min and resealed. All potentials were reported relative to the Ag pseudo-reference. The conductivity of the polymer electrolytes was determined by a.c. impedance in the frequency range from 0.1 Hz to 1 MHz at a perturbation signal of 5 mV. The electrochemical cell for conductivity measurements is illustrated in Fig. 1; the polymer electrolyte was sandwiched by two parallel Pt electrodes in a sealed glass cell. The area and distance apart of the Pt electrodes were 0.25 cm^2 and 0.5 cm, respectively.

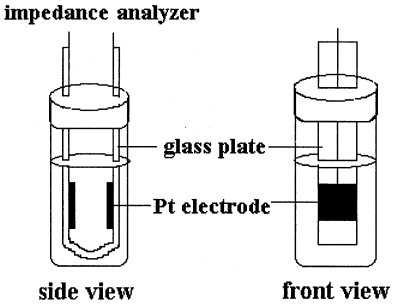

Fig. 1 Scheme of the electrochemical cell for conductivity measurements

Result and discussion

Determination of diffusion coefficients of PMo_{12}-Co nanoparticles

Determination of the diffusion coefficient (D_{app}) for electroactive species in polymer electrolytes has been described, usually using chronoamperometry at a microdisk electrode according to Shoup and Szabo [15, 16, 17]:

$$i = 4nFD_{app}cr\left\{0.7854 + 0.8862\tau^{-1/2} + 0.2146 \exp\left(-0.7823\tau^{-1/2}\right)\right\} \quad (1)$$

$$\tau = 4D_{app}t/r^2 \quad (2)$$

$$i = \pi^{1/2}nFD_{app}^{1/2}cr^2/t^{1/2} + 4nrFDc \quad (0.01 < \tau < 100) \quad (3)$$

where c is the concentration of the electroactive species, r is the microelectrode radius; the other terms have their usual meanings. In this method, the diffusion limiting current at the potential step is given by Eq. 3; the intercept b and slope k can be obtained from the plot of i vs. $t^{-1/2}$:

$$D_{app} = \pi(br/4k)^2 \quad (4)$$

D_{app} can be determined by Eq. 4 without prior knowledge of the reaction electron number. In the present work, D_{app} was determined and each diffusion coefficient was estimated at four scan rates to improve the statistics.

Determination of the interaction in the PEG-$LiClO_4$-PMo_{12}-Co system

Figure 2 shows the FT-IR spectra of the polymer electrolytes. The bands for C-O-C symmetric and asymmetric stretching vibrations observed at ~1100 cm^{-1} for PEG were reported previously [18, 19]. In our study the C-O-C bands of pure PEG-600 are at 1108.7 cm^{-1} (Table 1), but when $LiClO_4$ is added in PEG-600 the position of the C-O-C maximum stretch decreases to

1101.1 cm^{-1}. In this case, PEG chains are coiled around the Li^+ cations which separates them from the ClO_4^- counter anions, indicating that the C-O-C stretch connects with the formation of the transient cross-links between Li^+ and C-O-C of the PEG, these cross-links leading to a stiffening of the polymer chain with the C-O-C stretch shifting to a lower wavenumber. The addition of PMo_{12}-Co nanoparticles results in a variation in the position of the C-O-C stretching maximum from 1101.2 to 1105.6 cm^{-1}. The 815.3 cm^{-1} bands associated with Mo-O_b stretching of PMo_{12}-Co are observed at 813.2 cm^{-1} in PEG-600 containing $LiClO_4$ [20, 21], which indicates the change of the ether oxygen and the Mo-O_b environments. Owing to the large surface area, PMo_{12}-Co nanoparticles can prevent local PEG chain reorganization, resulting in a high degree of disorder at ambient temperature [22]. Moreover, the competition of the nanoparticles in the reaction of Li^+ with ClO_4^- and ether oxygen reduces the number of transient cross-links of the PEG chains and leads to the variation of wavenumber for C-O-C and Mo-O_b in the IR spectra.

Dependence of D_{app} on the temperature of the PMo_{12}-Co nanoparticles in PEG with different molecular weights

Figure 3 shows a series of cyclic voltammograms (CVs) of 5.0 mM PMo_{12}-Co in PEG-600 containing $LiClO_4$ (O/Li = 100/l) at different scan rates. The CVs exhibit three-step redox waves of PMo_{12}-Co denoted by A, B, and C, with the midpoint potentials E_{mid} of 0.02, –0.11, and –0.39 V, respectively, where $E_{mid} = (E_{pc} + E_{pa})/2$ and E_{pc} and E_{pa} are the cathodic and anodic peak potentials. The CVs of PMo_{12}-Co in PEG are similar to that in organic solvents which exhibit three one-electron waves with low Li^+ concentration [23, 24]. Waves A and B exhibit one-electron processes and the electron number of wave C is nearly 1 in PEG. Determination of D_{app} is

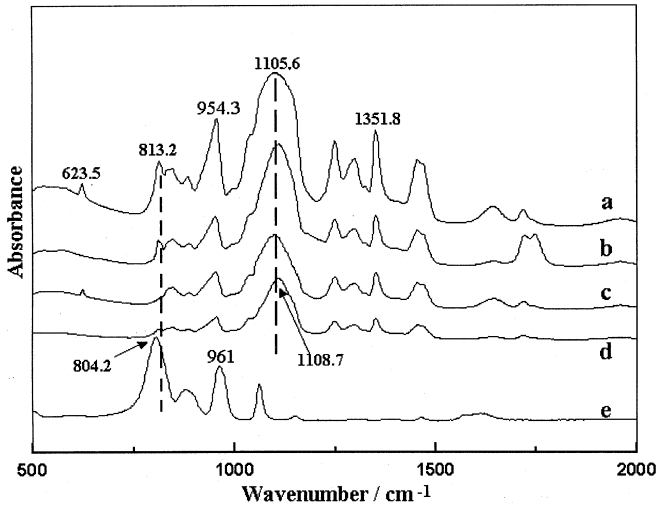

Fig. 2 FT-IR spectra of polymer electrolyte systems in the spectral region between 500 and 2000 cm^{-1}: (*a*) PEG-600-$LiClO_4$-PMo_{12}-Co; (*b*) PEG-600-PMo_{12}-Co; (*c*) PEG-600-$LiClO_4$; (*d*) pure PEG-600; (*e*) pure PMo_{12}-Co

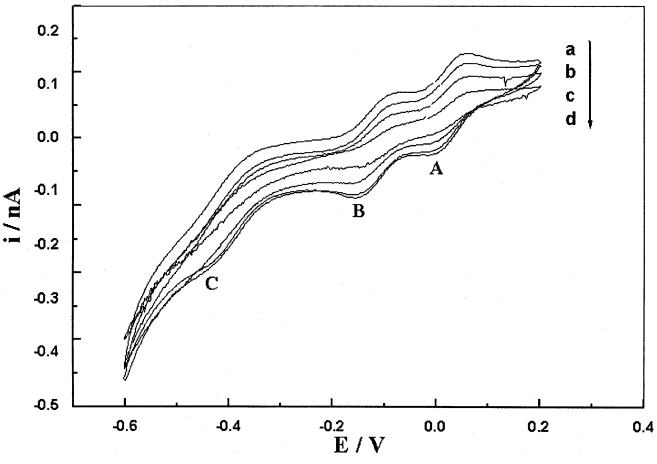

Fig. 3 Cyclic voltammograms of 5.0 mM PMo_{12}-Co nanoparticles in PEG-600 containing $LiClO_4$ (O/Li = 100/1) at different scan rates: (*a*) 100 mV/s; (*b*) 50 mV/s; (*c*) 30 mV/s; (*d*) 10 mV/s

Table 1 FT-IR wavenumbers (cm^{-1}) for the PEG- $LiClO_4$-PMo_{12}-Co system[a]

PMo_{12}-Co	PEG-600	PEG-600-$LiClO_4$	PEG-600-PMo_{12}-Co	PEG-600-$LiClO_4$-PMo_{12}-Co	Assignment
–	1108.7 vs	1101.1 vs	1108.2 vs	1105.6 vs	C-O-C stretching
1061.4 m	–	–	–	–	P-O stretching
961.0 s	–	–	–	–	Mo-O_d stretching
–	952.2 m	952.3 m	954.1 m	954.3 m	C-O and CH_2 rocking, C-O-C stretching
–	886.1 vw	886.3 vw	884.4 vw	886.5 vw	C-O and CH_2 rocking, C-O-C stretching
877.7 m	–	–	–	–	Mo-O_c stretching
–	846.3 w	845.3 w	845.9 w	845.2 w	CH_2 rocking
–	–	–	815.3 s	813.2 s	Mo-O_b stretching
804.2 vs	–	–	–	–	Mo-O_b stretching
–	–	623.4 vw	–	623.5 vw	ClO_4^- stretching

[a]Approximate relative intensities: vs, very strong; s, strong; m, medium; w, weak; vw, very weak

based on the potential interval of wave B using chronoamperometry.

The temperature dependence on D_{app} of PMo_{12}-Co nanoparticles in PEG with different molecular weights is shown in Fig. 4. A sharp discontinuity of D_{app} vs. T curves occurs in both PEG-1000 and PEG-2000 at around 30 and 50 °C, respectively. However, D_{app} vs. T curves for PEG-400 and PEG-600 show no discontinuities because they are viscous liquids at the experiment temperature intervals and no crystalline state of the polymers exits. The diffusion of PMo_{12}-Co nanoparticles through entirely an amorphous polymer in PEG-400 and PEG-600 is confirmed by IR spectra and the soft wax melting temperature of the polymer electrolytes (T_m; Table 2). As shown in Fig. 2, the shoulder of curve d is not observed at 1345 and 1360 cm^{-1}, which are assigned to C-H rocking vibration modes of crystalline ether oxygen units [25, 26], but there is an obvious peak at 1352 cm^{-1} corresponding to C-H rocking vibration modes of the amorphous state. The result shows that there is no phase change of the PEG with low molecular weight. Obviously, in Fig. 4 the discontinuity in the D_{app} vs. T curves for PEG-1000 and PEG-2000 coincides with the formation or dissolution of the ordered regions, which impede molecular diffusion and ionic mobility. Diffusion variations of PMo_{12}-Co nanoparticles are dependent on temperature, especially on the PEG phase state, which reflects the dynamics of the PEG chain segmental mobility [27].

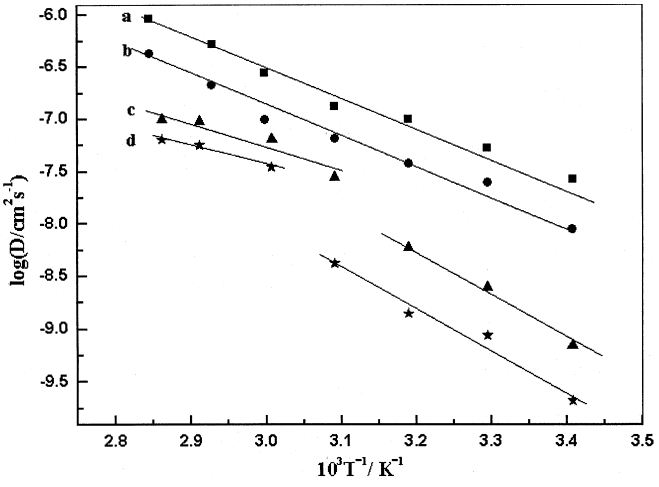

Fig. 4 Temperature dependence on diffusion coefficient for PMo_{12}-Co nanoparticles in polymer electrolytes with different PEG molecular weights: (*a*) PEG-400; (*b*) PEG-600; (*c*) PEG-1000; (*d*) PEG-2000

Dependence of D_{app} on concentration of PMo_{12}-Co nanoparticles in PEG-600

The results in Fig. 5 show that D_{app} in PEG-600 appears to be insensitive to the concentration of PMo_{12}-Co nanoparticles in the range from 2.5 to 5 mM, but at high concentrations of PMo_{12}-Co nanoparticles then D_{app} undergoes a substantial decrease; the changes follow the equation [28]:

$$D_{app} = D(0)\exp(-\beta W_f) \quad (5)$$

where W_f is the weight fraction of the PMo_{12}-Co nanoparticles, $D(0)$ is D_{app} at $W_f = 0$, and β is a constant. Equation 6 can be changed to the following form:

$$D_{app} = D(0)\exp(-yc) \quad (6)$$

where y is a constant and c is the concentration of PMo_{12}-Co nanoparticles. Equation 6 is analyzed in

Table 2 Extracted parameters for the circuit elements evaluated by fitting the impedance data to the equivalent circuit according to Fig. 7

	T_m (°C)	CPE		R_b (kΩ)	C_g (pF)	Conductivity (S cm^{-1})	Standard errors for conductivity
		A	n				
PEG-600	–	7.4×10^{-11}	0.73	12,970	7.21	1.54×10^{-7}	1.4
PEG-600-2.5 mM PMo_{12}-Co	–	8.4×10^{-10}	0.63	11,660	7.63	1.71×10^{-7}	0.7
PEG-600-$LiClO_4$	10.1	5.3×10^{-6}	0.71	15.71	39.9	1.27×10^{-4}	0.3
PEG-600-$LiClO_4$-2.5 mM PMo_{12}-Co	1.2	7.6×10^{-6}	0.77	10.55	38.6	1.90×10^{-4}	0.9
PEG-600-$LiClO_4$-5.0 mM PMo_{12}-Co	2.4	2.7×10^{-6}	0.73	9.48	38.7	2.11×10^{-4}	5.6
PEG-600-$LiClO_4$-25 mM PMo_{12}-Co	2.1	2.9×10^{-6}	0.71	10.63	38.2	1.88×10^{-4}	1.7
PEG-600-$LiClO_4$-50 mM PMo_{12}-Co	1.7	8.2×10^{-6}	0.77	10.91	39.1	1.83×10^{-4}	1.1
PEG-400-$LiClO_4$-5.0 mM PMo_{12}-Co	–12.8	3.4×10^{-5}	0.89	7.91	38.5	2.53×10^{-4}	0.3
PEG-1000-$LiClO_4$-5.0 mM PMo_{12}-Co	28.2	6.6×10^{-9}	0.57	486	15.3	4.12×10^{-7}	2.9
PEG-1000-$LiClO_4$	–	2.8×10^{-11}	0.53	20,430	2.46	9.62×10^{-8}	3.1
PEG-2000-$LiClO_4$-5.0 mM PMo_{12}-Co	50.2	–	–	–	–	–	–

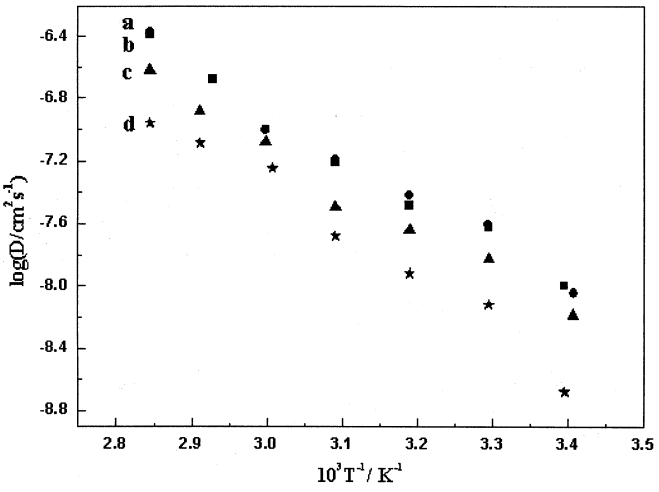

Fig. 5 Temperature dependence on diffusion coefficient for different PMo_{12}-Co nanoparticle concentrations in a polymer electrolyte containing $LiClO_4$ (O/Li = 100/1): (*a*) 2.5 mM; (*b*) 5 mM; (*c*) 25 mM; (*d*) 50 mM

terms of free volume theory, which is the simplest way to understand polymer segmental mobility. It states that as the temperature increases, the expansivity of the material produces local empty space, free volume, into which ionic carriers, solvated molecules, or polymer segments can move [29]. It is concluded that PEG can strongly solvate ions by dipolar or coordinating interactions; such interactions may reduce the chain segmental mobility according to the solute or electrolyte concentrations. The effect on segmental mobility is noticeable only when the concentration is appreciably high and the small concentrations of PMo_{12}-Co nanoparticles produce negligible changes in D_{app}.

Another important point is that the transport of electrochemical charge to and from the electrode can occur not only by physical diffusion of the oxidized and reduced forms of electroactive species but also by electrons hopping between them. The apparent diffusion coefficient, D_{app}, of an electroactive species is given by the Dahms-Ruff equation [30, 31]:

$$D_{app} = D_{phys} + k_{ex}\delta^2 c/6 \tag{7}$$

where D_{phys} is the physical diffusion coefficient, k_{ex} is the electron hopping rate constant, δ is the center-to-center intersite distance at electron transfer, and c is the total concentration of the electroactive probe. In order to detect whether the D_{app} values obtained reflect only physical diffusion or include a contribution from electron hopping, the dependence of D_{app} of the PMo_{12}-Co nanoparticles was evaluated in PEG since the contribution of electron hopping should be proportional to the probe concentration according to Eq. 7. As shown in Fig. 5, it is easy to find that D_{app} decreases when the PMo_{12}-Co nanoparticle concentration increases from 5 to 50 mM, so it can be concluded that the contribution of electron hopping in the D_{app} values may be negligible in PEG.

Dependence of conductivity on PMo_{12}-Co nanoparticles in PEG

In order to study the bulk resistance and electrical behavior of the polymer electrolytes, the impedance data are analyzed using equivalent circuit software. Figure 6 shows the real (Z') versus imaginary (Z'') parts of the complex impedance plot with Pt electrodes at ambient temperature; the inset is the equivalent circuit. The impedance data of Pt/polymer electrolyte/Pt structures are fitted and shown in Fig. 6 (solid line); it can be seen that the theoretical line calculated from the estimated values shows a good correlation with the experiment data. The extracted parameters for the circuit elements are summarized in Table 2. In Fig. 6 the semi-circle in the high-frequency region represents the characteristics of the bulk geometrical capacitance (C_g) and bulk resistance (R_b) of the polymer electrolyte; the inclined straight line in the low-frequency region reflects the effect of the polymer electrolyte/electrode interface for which constant phase elements (CPEs) are used to represent the equivalent circuit [32, 33]. When the slope of the straight line is different from 45°, it can be interpreted that there is inhomogeneous diffusion combined with a charge transfer reaction. The impedance of the CPEs is given by an empirical formula [34, 35]:

$$Z_{CPE} = A(j\omega)^{-n} \tag{8}$$

$$\alpha = (1-n)\frac{\pi}{2} \tag{9}$$

where A is the inverse of the capacitance only when $n = 1$, and n is related to α (the deviation from the vertical line in Nyquist impedance plot); $n = 1$ indicates a perfect capacitance, and a lower n value directly reflects the roughness of the electrode used.

Table 2 gives the R_b and conductivity values calculated by the equivalent circuit, and Fig. 7 shows the a.c.

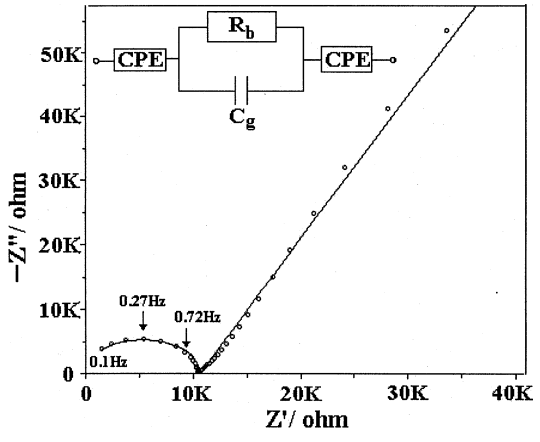

Fig. 6 A.c. impedance spectrum for the Pt/PEG-600-$LiClO_4$-5 mM PMo_{12}-Co/Pt system at ambient temperature. The data are limited to the frequency range from 1 Hz to 1 MHz; the *solid line* represents the fitted response of the equivalent circuit (shown in the *inset*)

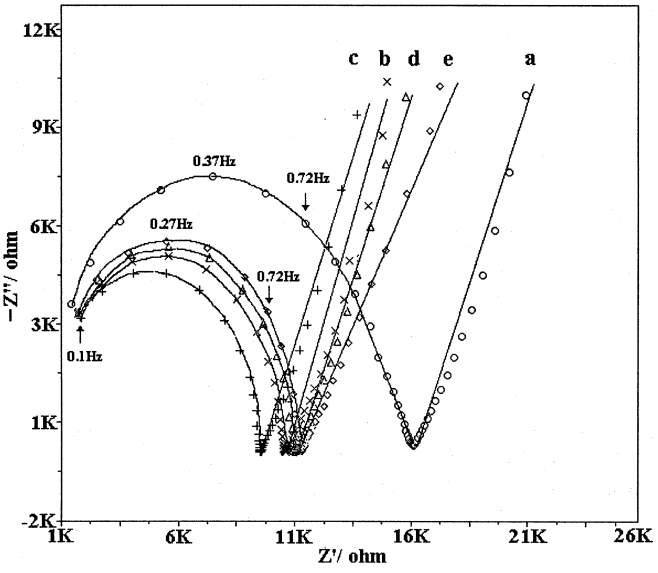

Fig. 7 A.c. impedance spectra for a symmetric Pt/polymer electrolyte/Pt system at ambient temperature with different concentrations of PMo_{12}-Co nanoparticles (O/Li = 100/l); the *solid line* represents the fitted response of the equivalent circuit. (*a*) PEG-600-$LiClO_4$; (*b*) PEG-600-$LiClO_4$-2.5 mM PMo_{12}-Co; (*c*) PEG-600-$LiClO_4$-5 mM PMo_{12}-Co; (*d*) PEG-600-$LiClO_4$-25 mM PMo_{12}-Co; (*e*) PEG-600-$LiClO_4$-50 mM PMo_{12}-Co

impedance plot of Pt/polymer electrolytes/Pt with different concentrations of PMo_{12}-Co nanoparticles. From Fig. 7 and Table 2 it can be easily found that the ionic conductivity of PEG-600 containing $LiClO_4$ only (O/Li = 100/1) is 1.27×10^{-4} S cm^{-1}, and an obvious increase in conductivity is observed after the addition of the PMo_{12}-Co nanoparticles. The increase in conductivity here cannot be ascribed to the change of phase state since PEG-600 is a completely amorphous phase at ambient temperature, and also cannot be ascribed the conductivity of PMo_{12}-Co nanoparticles for there is a slight increase in conductivity upon the addition of PMo_{12}-Co nanoparticles to pure PEG (Table 2). It should be explained by interactions in the systems, because the addition of PMo_{12}-Co nanoparticles results in a variation of the interactions among PEG-$LiClO_4$, $LiClO_4$-PMo_{12}-Co, and PEG-PMo_{12}-Co. PMo_{12}-Co nanoparticles might compete against ClO_4^- and ether oxygen for Li^+, which leads to a reduction of the number of transient cross-links of the PEG chains, and forms a highly conductive layer covering the surface of the PMo_{12}-Co [36, 37]. Such a structure modification would provide Li^+ conducting pathways at the PMo_{12}-Co surface. At the same time, polyoxometalate nanoparticles will diffuse under the applied electric field, that is, the conductivity the pathway is by mobility, which is an efficient improvement of the ionic conductivity.

It is interesting to find in Fig. 7 and Table 2 that when the concentration of PMo_{12}-Co nanoparticles increases from 2.5 to 5 mM, the conductivity of the polymer electrolyte also increases from 1.90×10^{-4} S cm^{-1} to 2.11×10^{-4} S cm^{-1}. However, at high concentrations of PMo_{12}-Co nanoparticles the ionic conductivities are slightly lower as compared to those at low concentrations. The conductivities of PEG-600-$LiClO_4$-PMo_{12}-Co systems have the sequence $5 > 2.5 > 25 > 50$ mM. The reason is that at low concentrations the conductivity pathway increases with an increase in PMo_{12}-Co nanoparticle concentration, so the conductivity is enhanced, while at the high concentration the main effect on the conductivity may relate to the viscosity change of the polymer electrolytes, but not the conductivity pathway formed by the nanoparticles. According to the Stokes-Einstein equation [38]:

$$D = kT/6\pi r\eta \tag{10}$$

where k is the Boltzmann constant and r is the hydrodynamic radius of the diffusion species. When the PMo_{12}-Co nanoparticle concentration substantially increases, η of the polymer electrolytes also increases, the diffusion of PMo_{12}-Co and Li ions decrease according to Eq. 8, so the conductivity decreases. The variation tendency of the conductivity for different molecular weight PEGs may be explained in a similar way to the viscosity.

Conclusions

PMo_{12}-Co nanoparticles show three redox couples in PEG. Microelectrodes were used to determine the diffusion coefficient of α-Keggin-type PMo_{12}-Co nanoparticles in PEG of four molecular weights. Diffusivity coefficient variations of PMo_{12}-Co are dependent on temperature and the PEG phase state, which reflects the dynamics of the PEG chain segmental mobility. In low concentrations of PMo_{12}-Co nanoparticles, negligible changes of D_{app} in PEG-600 are shown; when the concentrations of PMo_{12}-Co are high, the effect on segmental mobility is noticeable, which can be understood in terms of free volume theory.

After the addition of PMo_{12}-Co nanoparticles, the maximum conductivity increases from 1.27×10^{-4} to 2.11×10^{-4} S cm^{-1}, which should be explained in terms of PEG-$LiClO_4$-PMo_{12}-Co interactions. PMo_{12}-Co nanoparticles lead to a reduction in the number of transient cross-links of the PEG chains, and form a highly conductive layer covering the surface of PMo_{12}-Co. Such a structural modification will provide Li^+ with efficiently conducting pathways at the PMo_{12}-Co surface. To summarize, the improvement in conductivity is a result of PEG, salt, and nanoparticle interactions.

Acknowledgements This project was supported by the National Natural Science Foundation of China (no. 20075028).

References

1. Gómez-Romero P (2001) Adv Mater 13:163
2. Coronado E, Gomez-Garcia JC (1998) Chem Rev 98:273
3. Lira-Cantú M, Gómez-Romero P (1998) Chem Mater 10:698

4. Croce F, Appetecchi GB, Persi L, Scrosati B (1998) Nature 394:456
5. Xu W, Deng ZH, Zhang XZ, Wan GX (1998) J Solid State Electrochem 2:257
6. Morales E, Acosta JL (1999) Electrochim Acta 45:1049
7. Kato KI, Ito-Akita K, Ohno H (2000) J Solid State Electrochem 4:141
8. Best AS, Ferry A, MacFarlane DR, Forsyth M (1999) Solid State Ionics 126:269
9. Bruce PG, Vincent CA (1993) J Chem Soc Faraday Trans 89:3187
10. Geng L, Reed RA, Longmire M, Murray RW (1987) J Phys Chem 91:2908
11. Hatazawa T, Terrill RH, Murray RW (1996) Anal Chem 68:597
12. Hyk W, Ciszkowska M (2000) J Electrochem Soc 147:2268
13. Audebert P, Divisia-Blohorn B, Cohen-Addad JP (1997) Polymer Bull 39:225
14. Huang RD, Li J, Wang EB (2002) Chem Commun (revised)
15. Shoup D, Szabo A (1982) J Electroanal Chem 140:237
16. Longmire ML, Watanabe M, Zhang H, Wooster TT, Murray RW (1990) Anal Chem 62:747
17. Dong SJ, Gu NY, Zhou HF (1998) J Electroanal Chem 441:95
18. Roger F, Wei WH (1995) Macromolecules 28:1246
19. Matsuta S, Asada, Kitaura (2000) J Electrochem Soc 147:1695
20. Bi LH, Wang EB, Peng J, Huang RD, Xu L, Hu CW (2000) Inorg Chem 39:671
21. Kunio F, Hiroatsu M (1995) J Mol Struct 350:215
22. Croce F, Curini R, Martinelli A, Persi L, Ronci F, Scrosati B, Caminiti R (1999) J Phys Chem B 103:10632
23. Himeno S, Qsakai T, Saito A, Maeda K, Hori T (1992) J Electroanal Chem 337:371
24. Himeno S, Takamoto M, Ueda T (2000) J Electroanal Chem 485:49
25. Bernson A, Lindgren J, Huang W, Frech R (1995) Polymer 36:4471
26. Dissanayake M, Frech R (1995) Macromolecules 28:5312
27. Wooster TT, Longmire ML, Zhang H, Watanabe M, Murray RW (1992) Anal Chem 64:1132
28. Watanabe M, Longmire ML, Murray RW (1990) J Phys Chem 94:2614
29. Ratner MA, Shriver DF (1988) Chem Rev 88:109
30. Dahms H (1968) J Phys Chem 72:362
31. Ruff I (1970) Electrochim Acta 15:1059
32. Venkateswarlu M, Narasimha K, Reddy, Rambabu B, Satyanarayana N (2000) Solid State Ionics 127:177
33. Qian XM, Gu NY, Cheng ZL, Yang XR, Wang EK, Dong SJ (2001) J Solid State Electrochem 6:8
34. Ferloni P, Mastragostino M, Meneghello L (1996) Electrochim Acta 41:27
35. Macdonald J (1987) Impedance spectroscopy. Wiley, New York
36. Przyluski J, Siekierski M, Wieczorek W (1995) Electrochim Acta 40:101
37. Wieczorek W, Lipka P, Zukowska G, Wycislik H (1998) J Phys Chem B 102:6968
38. Baril D, Michot C, Armand M (1997) Solid State Ionics 94:35